to show whether such displacements are actually present in metals showing the resistance minimum at very low temperatures.

The type of atomic displacement which we have just described is simply a frozen-in longitudinal elastic wave whose wavelength is twice the spacing of the planes. Traveling elastic waves could have similar effects; and waves of longer wavelength would subdivide the Brillouin zone into smaller sections, as we have described in our discussion of CuAu. It is obvious that certain elastic waves, producing the energy gap just at the edge of the filled levels in the Brillouin zone, can result in a depression of electronic energy, just as we have described in other cases, and so can in principle stabilize an interaction between the elastic wave and the electronic wave functions. This is presumably one way to describe the effect which Bardeen[6] and Fröhlich[7] have used to explain superconductivity. As they have pointed out, the electronic wave functions whose energy change is significant are those just below the top of the Fermi distribution, and the elastic waves concerned are those whose propagation vectors are such as to cause energy discontinuities at the Fermi level. The energy discontinuity, as shown in Fig. 1(b), results in a very high curvature of the curve of energy *vs* propagation constant, and hence in a very small effective mass of the electrons just at the top of the lower band, which Bardeen correlates with an explanation of superconductivity in terms of a very high diamagnetism. The low superconducting transition temperature could be associated with the excitation of electrons into the upper band, much as we have suggested in the case of Au and the conductors showing a resistance minimum. If the suggestions of these writers regarding superconductivity should turn out to be correct, we thus see that there is considerable analogy between this phenomenon and the superlattice which we have been discussing.

I am greatly indebted to Professor B. E. Warren for pointing out the interesting superlattice effects taken up in this paper.

[6] J. Bardeen, Phys. Rev. **79**, 167 (1950); **80**, 567 (1950); **81**, 469 (1951); **81**, 829 (1951).
[7] H. Fröhlich, Proc. Phys. Soc. (London) **A63**, 778 (1950); Phys. Rev. **79**, 845 (1950); Proc. Phys. Soc. (London) **A64**, 129 (1951).

PHYSICAL REVIEW VOLUME 84, NUMBER 2 OCTOBER 15, 1951

Čerenkov Radiation from Protons and the Measurement of Proton Velocity and Kinetic Energy*

R. L. MATHER
Radiation Laboratory, University of California, Berkeley, California
(Received June 25, 1951)

High velocity protons ($\beta=0.68$) from the electrically deflected external beam of the 184-in. cyclotron were sent through materials of high index of refraction (crystalline silver chloride and extra dense flint glass), and light was detected photographically with the intensity and angular distribution characteristics of Čerenkov radiation as predicted by Frank and Tamm. This is the first observation of this radiation from particles other than electrons and proves that the radiation is not a function of the mass of the particle. The heavier particle suffers less scattering and change of energy in the material and allows the highly directional character of the radiation to be observed. By removing the effects of chromatic disperion with a suitable prism, the angular intensity distribution was reduced to a bell-shaped distribution about the predicted angle with a standard deviation of around fourteen minutes of arc. This approaches the delta-function distribution derived by Frank and Tamm. The light was shown to be totally plane polarized in the direction predicted by Frank and Tamm.

The possibility that the angular distribution of Čerenkov radiation could be used as an absolute measure of the velocity of the proton, and hence its energy, has been exploited and a device of great accuracy and simplicity has been developed for this measurement. The various effects which lower the resolution are discussed. An estimate of the accuracy with which the mean energy of the 340-Mev proton beam has been measured is ± 0.8 Mev.

I. INTRODUCTION

THE excellence of the original theoretical explanation[1–3] of Čerenkov radiation has overshadowed the experimental results[4–10] because scattering has prevented the unique properties of this radiation from being convincingly demonstrated. As a result there has

* This work was performed under the auspices of the AEC.
[1] I. Frank and I. Tamm, Compt. rend. acad. sci. U.R.S.S. **14**, 109 (1937).
[2] I. Tamm, J. Phys. (U.S.S.R.) **1**, 439 (1939).
[3] A more complete bibliography of Čerenkov radiation is found in UCRL report 1306, unpublished, which also has a more detailed treatment of the subject of this paper.

[4] P. A. Čerenkov, Compt. rend. acad. sci. U.R.S.S. **2**, 451 (1934).
[5] P. A. Čerenkov, Compt. rend. acad. sci. U.R.S.S. **20**, 651 (1938.)
[6] P. A. Čerenkov, Compt. rend. acad. sci. U.R.S.S. **21**, 116 (1938).
[7] P. A. Čerenkov, Compt. rend. acad. sci. U.R.S.S. **21**, 319 (1938).
[8] P. A. Čerenkov, Phys. Rev. **52**, 378 (1937).
[9] G. Collins and V. Reiling, Phys. Rev. **54**, 499 (1938).
[10] H. Wyckoff and J. Henderson, Phys. Rev. **64**, 1 (1943).

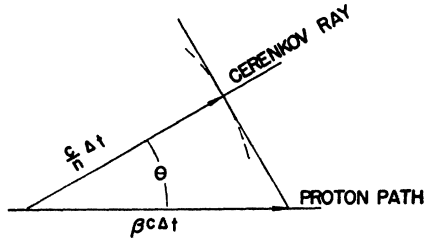

FIG. 1. Huygens' wavelet construction from which Eq. (1) may be derived.

been some tendency to confuse this type of radiation with that from an acceleration process such as bremsstrahlung,[9] although the distinction of it from ordinary fluorescence has been evident from the beginning.[4] The experimental results have also allowed some speculation about modifications of the theory.[11]

This radiation can be predicted as a solution of Maxwell's equations for a charged particle in uniform rectilinear motion through a medium in which the velocity of electromagnetic radiation is less than the particle velocity. It takes a form analogous to the shock wave from projectiles traveling in air faster than the velocity of sound. The existence of such a wave phenomenon, far from being uncommon, is observable in the bow wave from boats and can easily be observed in the family bathtub by drawing a pencil tip across the surface of the water.

The directional property of Čerenkov radiation is most readily seen from a Huygen's wavelet construction as shown in Fig. 1. The wavelets combine with each other to form a conical wave front symmetrical about the path of the particle. The normals to this wave front, or ray directions, make a constant angle θ with the path of the particle.

$$\cos\theta = 1/n\beta, \tag{1}$$

where c is the velocity of light in vacuum, n is the index of refraction of the medium with respect to vacuum, and βc is the velocity of the particle.

Since reinforcement is a phase phenomenon like refraction, it is the phase velocity which is important and n is strictly the index of refraction relative to vacuum. In the case of a dispersive medium both n and θ are functions of the frequency.

For $\beta n < 1$ the angle θ becomes imaginary, indicating that there is no radiation by this process.

Tamm's theory yields the following spectral intensity for the radiation. The change in the index of refraction over the visible region of the spectrum is usually small enough to allow an approximate calculation of the

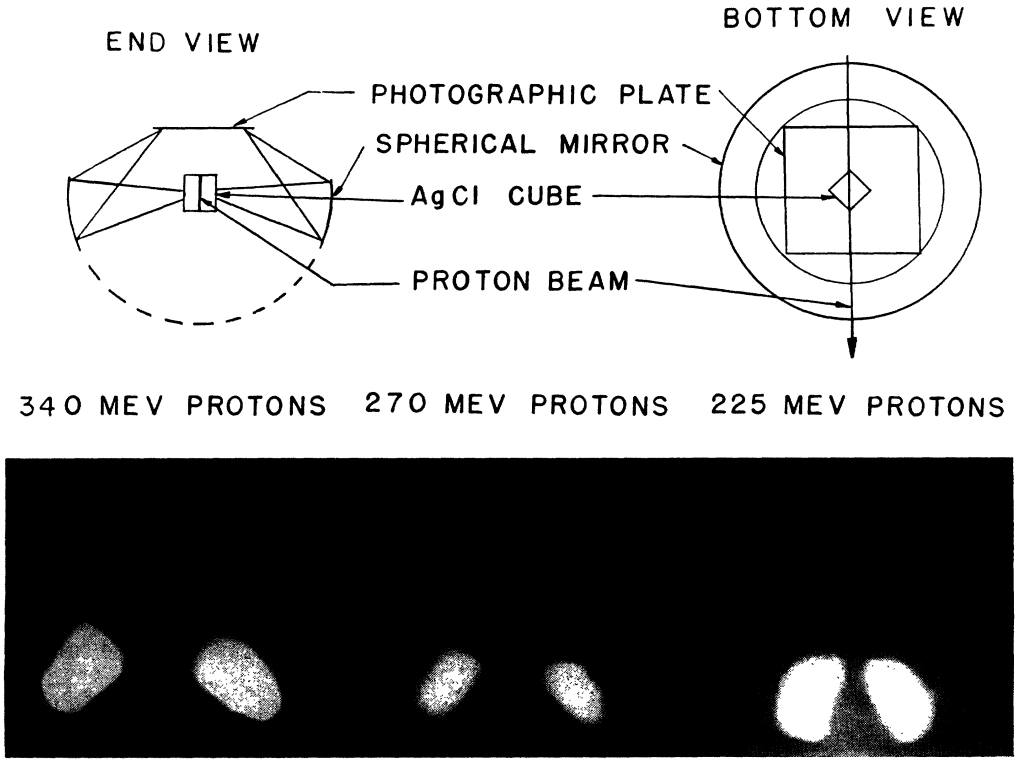

FIG. 2. Experimental arrangement and positive prints of the film showing Čerenkov radiation.

[11] Yin Yuan Li, Phys. Rev. **80**, 104 (1950), also Phys. Rev. **82**, 281 (1951).

total visible radiation to be made:

$$dN/dL=(z^2e^2/\hbar c^2)(1-1/n^2\beta^2)d\omega$$

quanta/unit path length

$$\approx 500 \sin^2\theta \text{ visible quanta/cm,} \quad (2)$$

where ze is the particle charge, $\hbar$ is $1/2\pi$ times Planck's constant, and ω is 2π times frequency.

If this is expressed in terms of energy distribution on a wavelength scale, the expression becomes

$$dW/dL=4\pi^2z^2e^2(\sin^2\theta/\lambda^3)d\lambda$$

radiated energy/unit path length, (3)

where λ is the wavelength of the radiation in vacuum.

This expression shows the radiation to be continuous in spectral distribution wherever $n\beta>1$. For the visible region the blue will receive emphasis both from the decrease in λ and from the usual increase in n and hence θ. The total energy lost by the particle in Čerenkov radiation is about 0.1 percent of that lost by other processes in the material; however, the intensity is high enough to observe in the visible region and dominates over other sources of radiation in the materials used here.

The polarization of the radiation is obvious from the observation that the particle has, and can radiate, only an azimuthal magnetic field and thus the electric vector of the radiation must lie in the plane determined by the point of observation and the path of the particle. The direction of the electric vector in the Čerenkov wave front points toward or away from the position of the particle according to whether the particle is negative or positive.

The foregoing considerations indicate the directional characteristics of the rays inside the material, but the observation of them requires that they escape and hence their directions will be altered by refraction at the surface. Since the radiation is formed throughout a large section of the materials, and near the boundary surface through which the light emerges, the problem of observing the initial direction of the radiation inside the material is complicated by spherical aberration unless the boundary surface is essentially plane. In the following instruments the light always emerges through a plane surface and the focusing of the rays, if any, is done in a separate process.

The deflecting apparatus of the cyclotron assures a well-collimated, nearly monoenergetic beam of 340-Mev, $\beta=0.68$, protons by the time it reaches the experimental area. The shielding around the cyclotron is sufficient that no special shielding of the light sensitive photographic film was needed. The cross section of the emerging beam can be varied, but since all the following instruments are sensitive only to a section of the beam about one centimeter square and there were no background problems, the cross section was made as large as possible unless considerations irrelevant to this experiment ruled otherwise.

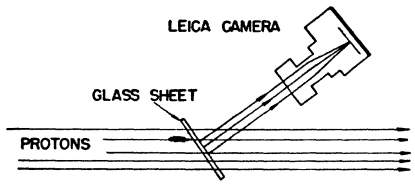

FIG. 3. Improved arrangement for viewing Čerenkov radiation.

The beam current density was about 2×10^{-11} ampere per square centimeter. This gave sufficient radiation for any of the following exposures to be made in less than one hour. Some of the later ones required only three minutes exposure. The short exposures are made possible by the use of very sensitive photographic emulsions and by concentrating the light to as small an area of film as possible.

II. INITIAL EXPERIMENTS

The successful experimental demonstration of Čerenkov radiation from protons was made with an instrument similar in principle, but somewhat simpler, to that used by Čerenkov,[7,8] Collins and Reiling,[9] and Wyckoff and Henderson.[10] The source, a one-centimeter cube of transparent silver chloride ($n=2.07$) with polished surfaces, was surrounded by a silvered spherical mirror which focused the light emerging in the horizontal plane to a ring at the position of the photographic film (see Fig. 2). Light emerging at large angles to the horizontal plane was prevented from reaching the mirror and the film by paper masks. Only those portions of the ring would be illuminated which lay in the direction in the horizontal plane in which light was emitted by the sample.

One diagonal of a horizontal face of the cube was placed parallel to the proton beam direction. There were four plane faces from which light could have been recorded. Light emerged from the two forward faces but not from the two rear faces (see Fig. 2). The velocity of the protons was reduced by placing copper foils in the beam and the angle between the intensity maxima decreased in accordance with the theory.

An order of magnitude calculation can be made for the intensity of the radiation from the sensitivity of the film and the exposure. This yields a figure of 105 quanta-cm compared to a theoretical value of 250 quanta/cm. This can be considered as agreement and

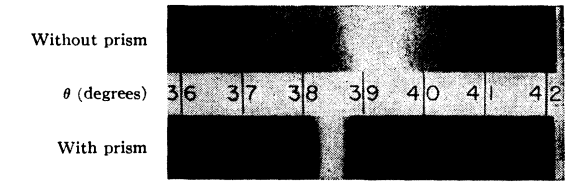

FIG. 4. Positive prints showing Čerenkov radiation as a function of an angle. Top—with equipment of Fig. 3. Bottom—with equipment of Fig. 7.

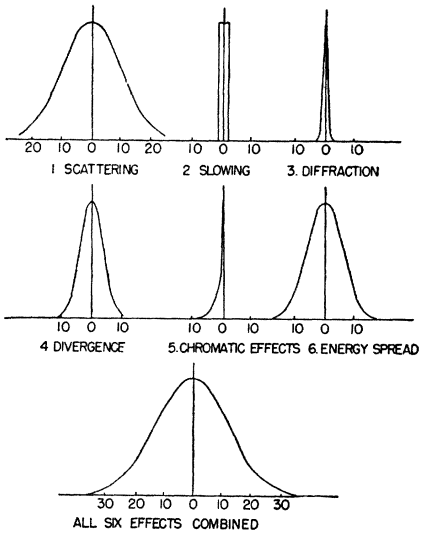

FIG. 5. Estimated angular intensity distribution of the achromatized Čerenkov rays (abscissas in equivalent minutes of arc in θ).

is additional proof that the observed radiation is Čerenkov radiation.

Were this radiation due to bremsstrahlung or any acceleration process of radiation, the intensity for electrons should be larger by the square of the mass ratio of 3.4×10^6, if one assumes the accelerating forces to be the same in both cases (i.e., electrical forces). The electron experiments of Čerenkov[6] and of Collins and Reiling[9] give intensities of the same order of magnitude as observed here.

III. IMPROVEMENT OF THE ANGULAR RESOLUTION

The theory predicts an angular intensity distribution as sharp as a delta-function for a given wavelength; accordingly the experiment was revised to see if anything approaching this sharpness could be observed. The optical system was improved by using optically ground surfaces on the material (now glass with $n=1.88$) and observing the light with a Leica camera which has a highly refined optical system (Fig. 3). Scattering and slowing down in the material was reduced by making it thin ($\frac{2}{3}$ mm). A picture taken with this apparatus is

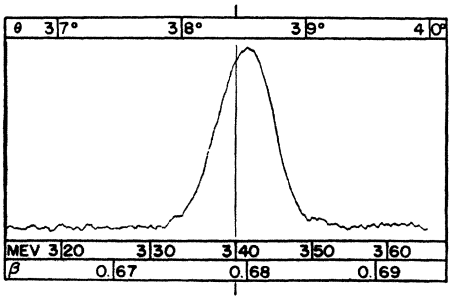

FIG. 6. Microphotometer trace of an achromatic Čerenkov radiation image.

shown in the upper portion of Fig. 4 with an accompanying scale in terms of θ.

Most of this width is the result of n, and hence θ, being a function of the wavelength of the radiation, which, from the theory and observation is a bluish-white spectrum. The camera looking into the glass surface will see a limited portion of a circular rainbow of light centered on the direction of the incoming proton beam with the blue outside and the red inside. A prism of the proper angle was ground whose dispersion would cancel the first-order dispersion of the Čerenkov rays. The rainbow viewed through this prism should coalesce to a narrow band of white light. A picture made through such a prism is shown in comparison to the previous picture (Fig. 4, bottom).

The breadth of this last image can be attributed to six effects: (1) scattering of the proton beam in the material, (2) change of velocity as material slows the protons down, (3) diffraction effects due to the finite

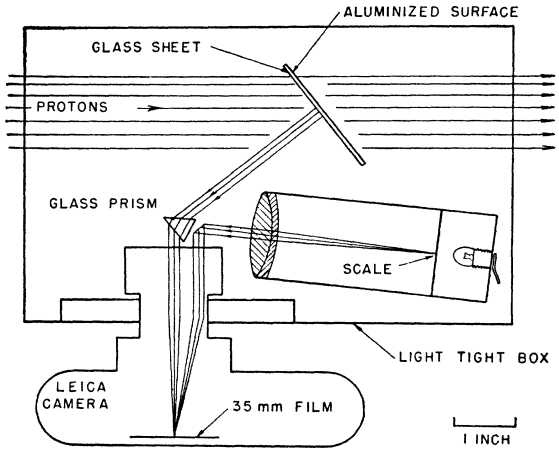

FIG. 7. Arrangement for the achromatic observation of the Čerenkov rays.

length of proton path in the glass, (4) the divergence of the incident proton beam, (5) second-order chromatic effects, and (6) the velocity spread of the incident proton beam.[12] Estimates of all these effects can be made and graphs of intensity *vs* angle for the individual effects and their combined effect are shown in Fig. 5. A microphotometer record of the Čerenkov image is shown in Fig. 6. If the ordinate of the record is converted to light intensity, the agreement is good. This result is quite in agreement with the delta-function angular distribution predicted by the theory of Frank and Tamm.

Taking the raw data with no corrections for any of the aforementioned effects, one can conclude that the radiation must be coherent with the particle over a path length of 0.01 cm, or the diffraction pattern alone

[12] Detailed discussions of these effects, a discussion of the combined results, and the possibilities of improvement will be found in the last portions of this paper.

would be larger than the observed width. This length would be on the order of a million atoms of the material or two hundred wavelengths of visible light.

Coherence of a slightly different sort is found in the completely plane polarized nature of the Čerenkov light. This was tested by fastening strips of polaroid across the camera film oriented at angles of 0, 70, 90, 110, and 180 degrees to the expected plane of polarization of the light. An exposure of 15 times the normal exposure still showed no indication of the Čerenkov image behind the strip oriented at 90 degrees to the plane of polarization, while the image behind the other strips indicated intense exposures. The ratio of exposures behind the 90 degree strip to that behind the 0- and 180-degree strips was less than 0.005, indicating total plane polarization in agreement with the theory.

FIG. 8. Energy measuring instrument. Left—normal position (aluminum foil removed from the light tight box of Fig. 8 to show interior construction). Right—inverted position.

IV. PROTON ENERGY MEASUREMENTS

A. Method and Apparatus

The resolution in θ obtainable with the achromatic arrangement opens the possibility of measuring the velocity and hence the kinetic energy of the protons in the beam using the relativistic equation:

$$E=\mu c^2\left(\frac{1}{(1-\beta^2)^{\frac{1}{2}}}-1\right)=\mu c^2\left(\frac{n\cos\theta}{(n^2\cos^2\theta-1)^{\frac{1}{2}}}-1\right), \quad (4)$$

where E is the kinetic energy and μ is the mass of the particle. Only two factors enter into this measurement —the angle θ between the proton path and the Čerenkov rays and the index of refraction of the glass. Both of these can be measured with high absolute accuracy, and a scale of β and Mev are shown in conjunction with the microphotometer trace.

The instrument used for the energy measurement furnished the pictures of Čerenkov radiation which have just been discussed. The diagramatic layout of the instrument is shown in Fig. 7. The glass in which the Čerenkov radiation is produced is shown in the proton beam. It is a thin sheet of extra dense flint glass ($n=1.88$) about $\frac{2}{3}$ of a millimeter thick with flat optically polished surfaces. The achromatizing prism is shown out of the beam and immediately in front of the Leica camera lens. If the Čerenkov rays were allowed to proceed in their original forward direction, the camera would have to be placed in the proton beam. To avoid this the surface of the glass sheet through which the beam emerges is aluminized and the Čerenkov rays are reflected back on themselves to emerge in the direction shown. A small projector projects an image of a scale on the film via a small mirror. This scale image is the reference point from which the angle at which the camera sees the Čerenkov radiation is measured. The camera is focused at infinity.

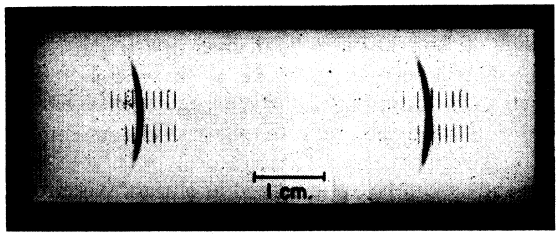

FIG. 9. A pair of Čerenkov images from which the beam energy may be determined (negative print).

The problem of relating the position of the image in the camera to the angle θ between the Čerenkov rays and the proton paths is simplified if both directions are measured separately relative to the normal to the aluminized surface of the glass.

B. Measurement of the Angle between the Mirror Normal and the Proton Beam Axis

Establishing the direction of the proton beam to within a few minutes of arc is difficult; however this can be avoided by taking two exposures and inverting the equipment between exposures (Fig. 8). A pair of such exposures is shown in Fig. 9. The average of the two positions of the Čerenkov rays will be, very accurately, the position that would have been obtained if the proton beam had been parallel to the axis about which the equipment was inverted. This approximation is better the more nearly the axis of inversion approaches the beam direction.

This inversion is carried out by mounting the instrument assembly of Fig. 7 on a platform whose hollow cylindrical end pieces, through which the beam passes, rest in the two "vee" supports as shown in Fig. 8. The instrument can then be turned in the kinematical bear-

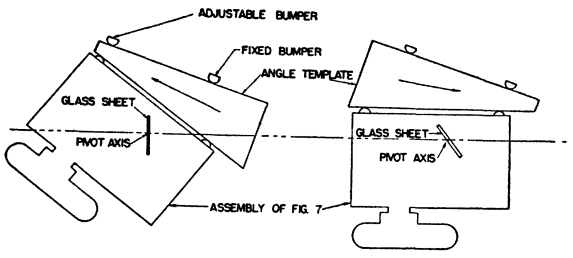

FIG. 10. Use of the angle template. Left—to adjust the bumper Right—to run.

ing thus provided. A latch will hold the equipment in any one of four positions 90 degrees apart.

The angle between the axis of inversion and the normal to the aluminized surface is accurately fixed by the use of precision angle templates. The assembly of Fig. 7 is supported on the platform by pivots which allow the assembly to be turned about an axis through the center of the glass sheet and perpendicular to the plane of Fig. 7. The platform and the assembly both carry two semicircular bumpers. A triangular steel template can be wedged between the two sets of bumpers and the angular position of the assembly with respect to the platform rigidly fixed.

The template is wedged in from one side and the position of one of the bumpers is adjusted so that the normal to the aluminized surface is parallel to the axis of inversion (Fig. 10, left). This is determined by viewing the image of a distant light source reflected by the aluminized surface with a telescope equipped with cross hairs. If the normal is parallel to the axis of inversion, the position of the image will not change when the instrument is inverted.

If the template is now wedged in from the other direction (Fig. 10, right) the angle between the normal to the mirror and the axis of inversion is exactly twice the angle of the template.

The angle templates were ground by standard precision machining techniques using a sine bar and gauge blocks. The amount of rotation of the assembly has been checked by viewing images of distant objects reflected in a mirror attached to the assembly and then measuring the angular separation of the objects seen in the two positions of the assembly with a surveyor's transit. The rotation was measured as $(38° 26.1')\pm 0.5'$. The machinist's value for the template was $(19° 13')$ $\pm 0.2'$.

C. Measurement of the Angle between the Čerenkov Rays and the Mirror Normal

The position of the film image can be related to the angle between the ray directions inside the glass and the normal to the aluminized surface by the following procedure. The camera back is removed and an assembly carrying a cross hair in the plane formerly occupied by the film is substituted. Light from a mercury vapor lamp is sent into the lens from behind the cross hair. An image of the cross hair passes through the lens, through the prism, and into the glass sheet, where it is finally reflected from the aluminized surface and retraces its path to form a real image in the plane of the cross hair. The light of the 5461A mercury green line is used (the achromatizing prism serves as a monochromator). The prism is set for minimum deviation and the cross hair is set so that its reflected image coincides with itself. The scale projector is turned on and the central line of the scale is adjusted to coincide with the position of the cross hair and its image.

TABLE I. Summary of estimated errors.

		$\Delta\beta$	ΔMev
Error in θ	$\pm 2.5'$	± 0.00040	± 0.6
Error in n	± 0.0003	± 0.00012	± 0.2
Error in reading	$\pm 1.6'$ in θ	± 0.00025	± 0.4
Total error		± 0.0005	± 0.8

The relation between the scale divisions on the film and direction as seen by the camera was measured by superimposing the scale on a picture of a distant scene and then measuring the angles between the apparent positions of the lines in the scene with a transit. The separation was found to be $61'$. Since the prism is at minimum deviation, it does not alter the apparent separation of the scale divisions in the region of the center of the scale. Because of refraction at the surface of the glass the angular separation of the rays inside the glass corresponding to one scale division is $61'$ divided by the index of refraction (since the rays are nearly normal to the surface and the angles of incidence and refraction equal their sines) or $32.4'$.

From this it is known that if an image of Čerenkov radiation is formed at the position of the center line of the scale by light of 5461A, the ray direction inside the glass was normal to the aluminized surface. If the image is not at the center line, one can interpolate the angle between the ray and the normal by reference to the scale divisions.

It must be understood that the foregoing discussion has applied to light of 5461A. If light of another wavelength is chosen for discussion, the index of refraction of both the prism and the glass sheet will be different. Using the data from this other wavelength, a given position on the scale combined with the change in deviation of the prism and the change in refraction at the surface of the glass will give a different Čerenkov angle θ. Disregarding small second-order effects, if the velocity of the proton is calculated using this new θ combined with the new index of refraction for the glass, one obtains the same proton velocity as would gave been calculated on the basis of the 5461A ray. This is another way of stating the achromatizing condition for the design of the prism. The 5461A mercury line was chosen for emphasis because it is readily available and its position in the spectrum corresponds to the wavelength of minimum second-order chromatic deviations for this particular instrument.

The absolute accuracy with which θ was measured has to be estimated as the sum of errors in a number of procedures already indicated. The estimate of the over-all accuracy in θ is $\pm 2.5'$.

D. Measurement of the Index of Refraction

The index of refraction of the glass sheet was known by measuring the index of refraction of a small prism ground from a section of the same piece of raw glass from which the sheet was ground. This measurement was the standard one of prism angle and minimum

deviation made on a precision spectrometer table. The results were corrected for the index of refraction of air. The index of refraction for the 5461A line relative to vacuum was 1.8796±0.0003.

E. Reading the Film

Because the width of the Čerenkov image is produced largely by effects thought to be symmetrical (except for the chromatic effects for which a correction of 1.7′ in θ is added), it is assumed that the midpoint of the image will correspond to the mean energy of the proton beam in the glass. The film is read with a microphotometer (the central parts of the scale lines have been left out to leave a clean path for the microphotometer) and the trace width is bisected at several heights and the average midpoint taken. This reduces the effect of random density fluctuations in the film.

The curvature of the Čerenkov image (mostly due to the properties of the achromatizing prism) and the problem of relating the microphotometer trace to the scale lines introduces errors in reading the trace. An estimated error in reading the film corresponds to 1.6′ in θ. Readings of the same film taken with two different types of microphotometers differed by less than 0.6′ in θ.

F. Results

The estimated errors in the measurement of θ and n and in reading the film are summarized in Table I along with their equivalents in velocity and kinetic energy. The estimates of errors quoted are admittedly not conservative. However the experimental results are in agreement with experiments which have been performed simultaneously with the use of this equipment.

For instance, the range energy relation has been checked by Mather and Segrè.[13] The results of their copper ranges are plotted in Fig. 11 along with the predicted range given by Aron, Hoffman, and Williams.[14] The disagreement is of the type and magnitude to be expected. The slope of the predicted range energy curve should be quite accurate, and using this it can be seen that the energy measurements are at least consistent (all angle adjustments were remade between runs).

A list of the energy measurements made with this apparatus is given in Table II. It corroborates something already known locally from range measurements, that the energy of the deflected beam from the 184-in. cyclotron is remarkably constant once the controls have been set, but a complete readjustment of the controls after an intervening duty on other experiments often results in a different energy.

V. RESOLUTION OF THE INSTRUMENT

The broadening effects graphically summarized in Fig. 5 will be discussed individually in the order of their appearance in Fig. 5. The results will then be combined for an expression of the over-all resolution and the possibilities for improving this resolution discussed. The amount of the correction for the chromatic effects will be calculated and the correction to be added or subtracted for the stopping power of instrument discussed. Lest the length of the discussion exaggerate their importance, it should be mentioned that both these corrections are about 0.43 Mev and the arbitrary and rough nature of some of the assumptions are quite unimportant for the experiment as a whole.

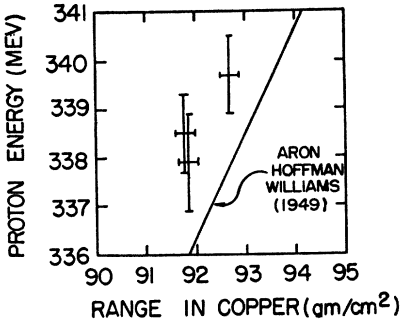

FIG. 11. Results of range energy measurements.

A. Scattering

A proton beam, whose direction is initially well defined, will interact with the atoms of the glass and the individual protons be deflected from the initial direction. The directions of the particles after traversing a layer of material will have a bell-shaped probability distribution with the following mean square angle:[15]

$$\langle\delta^2\rangle_{\text{Av}}=\frac{8\pi e^4Z^2z^2NX}{p^2v^2}\ln\frac{150p}{\mu cZ^{\frac{1}{3}}}, \tag{5}$$

where Z is the charge of the scattering nucleus; N is the number of nuclei per unit volume; ze is the charge of the

TABLE II. Mean energy of the electrically deflected proton beam from the 184-in. cyclotron as it enters the cave. (Rest energy of the proton taken as 938.17 Mev)(0.43 Mev added for stopping power of the instrument).

Date	Energy	Associated experiment
9/13/50	339.0	Range (Segrè)[a]
	338.5	
9/25/50	341.2	π^+ meson production (Cartwright)[b]
	341.3	
	341.5	
	341.3	
10/9/50	339.7	Range (Segrè)[a]
	339.4	
	339.3	
	339.2	
12/24/50	340.5	Range (Segrè)[a]
	340.6	
	340.5	

[a] See reference 13. [b] W. F. Cartwright, Phys. Rev. **82**, 461 (1951).

[13] R. Mather and E. Segrè, Phys. Rev. **84**, 191 (1951).

[14] Aron, Hoffman, and Williams, *Range Energy Curves*, United States Atomic Energy Commission, AECU-663, UCRL-121, (1949), unpublished.

[15] W. T. Scott, Phys. Rev. **76**, 212 (1949).

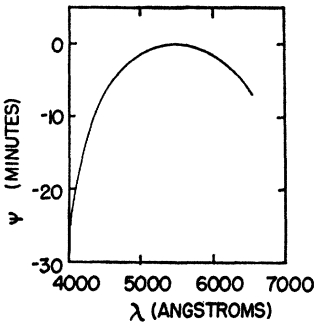

FIG. 12. Čerenkov ray angle as seen by the camera *vs* wavelength for $\beta=0.68$.

scattered particle; μ, p, v are the mass, momentum, and velocity of the scattered particle; and X is the depth of penetration in the material.

If the protons do not follow the path shown in Fig. 8, the instrument will be in error by an amount in θ equal to the angle of deviation projected on the plane of the paper. The mean square value of the projected scat-

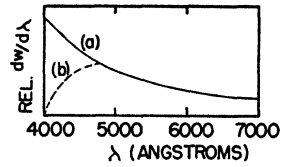

FIG. 13. Relative spectral density of Čerenkov radiation. (a) Calculated from Eq. (3). (b) Modified for absorption in the glass.

tering angle, η, is one half the mean square δ. Since the Čerenkov radiation is produced uniformly along the path and the mean square scattering angle is proportional to the penetration into the material, the mean square angle of the angular light intensity distribution will be one half of the mean square η for the total

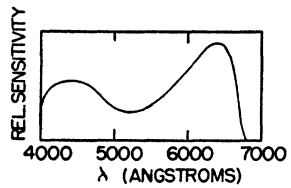

FIG. 14. Relative spectral sensitivity of Kodak Linograph Pan film.

thickness of the glass.

$$\langle\Delta\theta^2\rangle_{Av}=\tfrac{1}{2}\langle\eta^2\rangle_{Av}=\tfrac{1}{4}\langle\delta^2\rangle_{Av}. \quad (6)$$

The glass sheet had a thickness of 0.484 g/cm² in the beam direction. The properties of the material are listed in Table IV. Since the mean square scattering angle is proportional to Z^2, neglecting the logarithmic term, the rms Z of the composition was used. Substituting these data, one finds that the standard deviation of the angular intensity pattern due to scattering is 11 minutes of arc in θ.

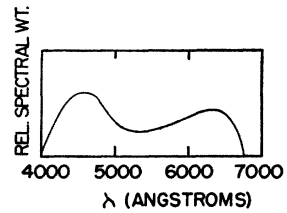

FIG. 15. Relative spectral weight of Čerenkov radiation.

B. Slowing

The particles suffer a loss of energy and a consequent reduction in velocity as they penetrate the glass. This means a continuous change of the Čerenkov angle and a square-topped angular intensity distribution from this source, symmetrical about a position corresponding to the proton energy in the center of the glass sheet.

An estimate of the energy loss in the instrument from range-energy calculations was 0.99 Mev. An attempted measurement of the stopping power gave 0.32 g/cm² copper equivalent, or 0.72 Mev. This discrepancy was deemed trivial for this experiment is comparison with other sources of error, and an arbitrary compromise was accepted of 0.38 g/cm² copper equivalent or an energy loss of 0.86 Mev. Accordingly, 0.43 Mev is added to or subtracted from the energy read from the peak of the microphotometer curve (after the correction for the chromatic effect) to give the energy of the proton beam entering or leaving the instrument.

The value of $d\theta/dE$ for this experiment is 3.94 minutes/Mev; consequently, $\Delta\theta=1.7$ minutes.

C. Diffraction

Diffraction broadens the image because only a finite length of wave front is obtained for the Čerenkov radiation. The limiting aperture is the length of the proton path in the material. The diffraction pattern would be the same as that from a slit of width $L\sin\theta$, where L is the proton path length in the glass. Since the radiation is not monochromatic, the total intensity distribution will have gaussian-like appearance with a standard deviation approximately given by

$$\Delta\theta=0.38\lambda_{\text{mean}}/nL\sin\theta. \quad (7)$$

For this experiment this is 0.68 minute, using $\lambda_{\text{mean}}=5000$A.

D. Divergence

The divergence of the original proton beam is a property of the cyclotron which is hard to measure. An estimate from the width of the beam defining collimating slits and the scattering in the vacuumtight window through which the beam emerges gives an rms projected divergence angle of about four minutes.

E. Chromatic Effects

The first-order chromatic effect in ψ, the ray direction as seen by the camera, is easily calculated on the assumption that the Čerenkov rays emerge nearly normal to the surface of the glass sheet and pass through the prism at nearly minimum deviation, providing both the sheet and prism are of the same type of glass. Equating this to zero gives an expression for

the prism angle α which achromatizes the system:

$$\frac{d\psi}{d\lambda}=\frac{d\psi}{dn}\frac{dn}{d\lambda}=\left[\frac{1}{(n^2\beta^2-1)^{\frac{1}{2}}}-\frac{2\sin\frac{1}{2}\alpha}{(1-n^2\sin^2\frac{1}{2}\alpha)}\right]\frac{dn}{d\lambda}=0, \quad (8)$$

$$\sin\tfrac{1}{2}\alpha=1/[n_0^2+4(n_0^2\beta_0^2-1)]^{\frac{1}{2}}. \quad (9)$$

Once the optical components have been produced, the index of refraction of the glass sheet and the deviation of the prism can be measured as a function of wavelength. By calculating the Čerenkov angle and the refraction at the surface of the glass, this can be combined with the prism deviation to give ψ with respect to wave length. Such a curve is plotted in Fig. 12. Here the 5461A ray has been taken in the calculations above, and ψ is arbitrarily taken to be zero for this ray.

The theoretical spectral distribution is modified for the transmission of the glass (it was quite yellowish) as in Fig. 13. This, times the spectral film sensitivity (Fig. 14), gives the spectral weight of the radiation forming the Čerenkov image (Fig. 15). Converting this from a function of wavelength to a function of ψ through the curve of Fig. 12 and multiplying by the inverse slope of this curve, one arrives at a curve of exposure intensity *vs* ψ as in Fig. 16. Since the curve of Fig. 12 goes through a maximum, the exposure curve has two branches and the total exposure intensity is the sum of the two.

This distribution is considerably narrower than that of the previously considered effects. However, it shifts the center of the image from the position of the 5461A line by the abscissa of the center of gravity of the exposure intensity curve, or by 3.2 minutes in ψ or 1.7 minutes in θ.

F. Energy Spread

The energy spread in the original proton beam has been estimated from the straggling observed in range measurements[13,16] as 1.8 Mev, although this estimate is of no great accuracy. This estimate is the standard deviation of a gaussian energy distribution. This energy spread would produce a gaussian light intensity distribution with a standard deviation of seven minutes in θ.

G. Combined Intensity Pattern

The individual effects which could cause the angular intensity distribution to be other than a delta-function have been calculated separately, and appropriate values for the widths have been given. These effects can be combined into a single distribution with a gaussian shape whose standard deviation is the square root of the sum of the squares of the individual widths (Table III).

This result can be compared with the microphotometer trace in Fig. 7. The apparent agreement is quite fortuitous, since the film characteristics are unknown. Using what handbook data are available, the microphotometer traces indicate a standard deviation of the line between 7 and 15 minutes in θ.

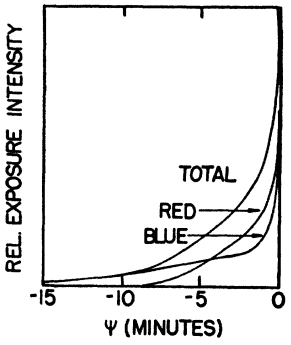

FIG. 16. Relative exposure intensity *vs* angle as seen by the camera (due to chromatic effects).

VI. IMPROVEMENT OF THE ENERGY RESOLUTION

If this calculated spread is converted to Mev, there is a standard deviation of 3.5 Mev. It will be interesting to see how much this energy resolution could be improved in future instruments and from what sources the improvements would come. For this purpose suitable analytic expressions can be developed for the various sources of poor resolution and combined to give an analytic expression for the energy resolution.

TABLE III. Estimated individual and combined angular widths.

	θ (minutes)	$(\Delta\theta)^2$
Scattering	11.0	121.0
Slowing	1.7	2.9
Diffraction	0.7	0.5
Divergence	4.0	16.0
Chromatic	0.9	0.8
Energy spread	7.0	49.0
Total	13.8	190.2

The effects of scattering and slowing will increase

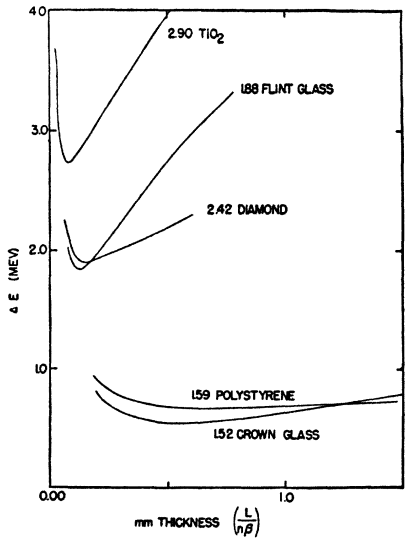

FIG. 17. Calculated energy resolution *vs* thickness of material for an instrument similar to the one in Fig. 7.

[16] C. J. Bakker and E. Segrè, Phys. Rev. **81**, 489 (1951).

TABLE IV. Properties of representative materials.

Material	Composition	n	θ ($\beta=0.68$)	ν	ρ	Z_{rms}	Z_{Av}	A_{Av}
Rutile ($\perp$ to optic axis)	TiO_2	2.90	59°	9.3	4.2	14.2	12.7	26.7
Diamond	C	2.42	52	57	3.5	6.0	6.0	12.0
Flint glass	$Pb_{20.9}Si_{19.4}O_{59.7}$	1.88	38	22	5.8	38.5	24.6	58.3
Polystyrene	C_8H_8	1.59	23	31	1.1	4.3	3.5	6.5
Crown glass	$Na_{6.4}K_{3.7}Ba_{0.8}B_{6.6}Si_{22.3}O_{60.3}$	1.52	14	64	2.5	11.4	10.1	20.7

with an increase of the proton path length in the material whereas the diffraction effects are proportional to the inverse of L. Thus there is an optimum thickness of the material for the best energy resolution.

The choice of the index of refraction cannot be separated from other properties of the material such as the reciprocal dispersion ν, the density ρ, and the atomic number and weight of the material; but, in general, substances whose indices are near the minimum for the production of Čerenkov radiation are favored because the decrease in $dE/d\theta$ reduces the effects of scattering and divergence on the energy resolution. If the index of refraction is too near the minimum, the chromatic effects due to dispersion begin to dominate and increase rapidly with decreasing index of refraction.

ΔE *vs* $L/n\beta$, the thickness of the sheet, is plotted for several substances listed in Table IV in Fig. 17. The optimum in L and the improvement with the low index materials is obvious. The outstanding qualities of polystyrene are not shown by the graph because the beam divergence is a prominent factor. In a divergenceless beam the energy resolution would be higher than any of the other materials shown and would be about 0.33 Mev.

The relative positions of these materials will change if other particles or other velocities are used. At the time of these experiments the protons used here had the largest heavy particle velocities that had ever been achieved. For lower velocities correspondingly higher indices of refraction are required, and the choice among suitable materials is very limited.

Fig. 17 shows that the present instrument with 2/3 mm of flint glass is rather far from the best possible energy resolution. The instrument design, however, was greatly simplified by the large value of θ obtained from the high index glass. The glass thickness would have been made less, but it was thought that the material would not have enough rigidity to hold its optical figure. Future instruments might well take advantage of the curves shown here by more careful and ingenious design.

I wish to acknowledge the suggestions and encouragement given in the early part of this experiment by Professors E. M. McMillan and W. K. H. Panofsky and in the later stages by Professor E. Segrè. The continuous support of Professor B. J. Moyer has made this experiment possible, and the assistance of the staff of the Radiation Laboratory and the Department of Physics has been most valuable.

I must also acknowledge the assistance of Mr. J. E. Gullberg, Professor of Metrology, Department of Zoology, who has allowed me to use his precision refractometer and offered valuable suggestions.

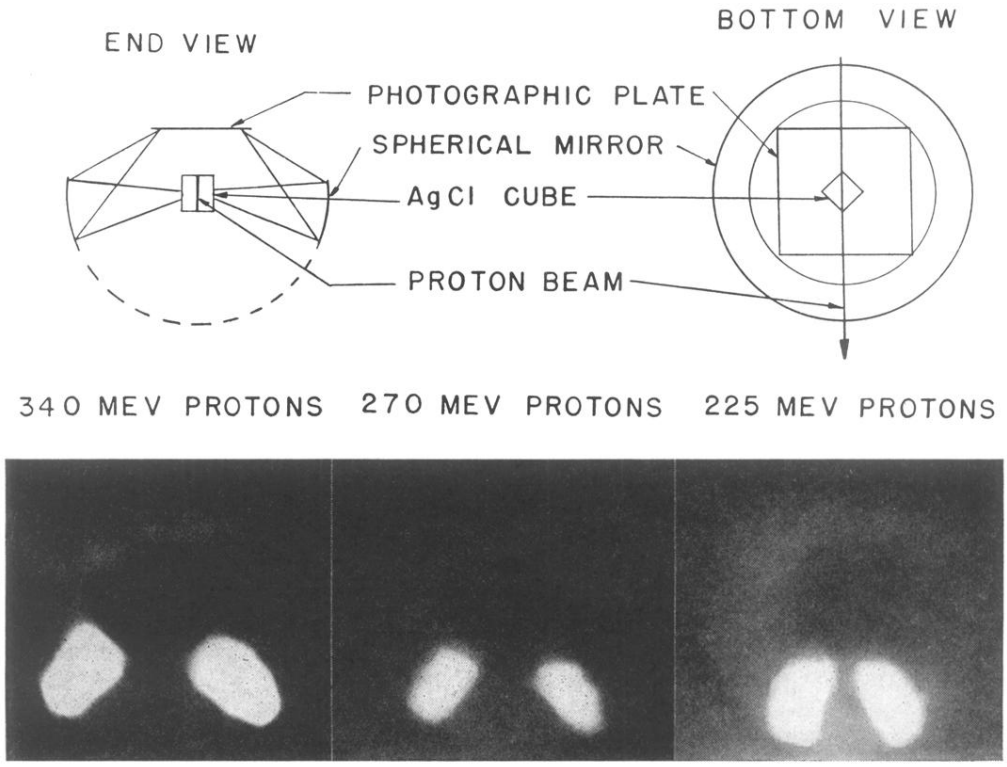

FIG. 2. Experimental arrangement and positive prints of the film showing Čerenkov radiation.

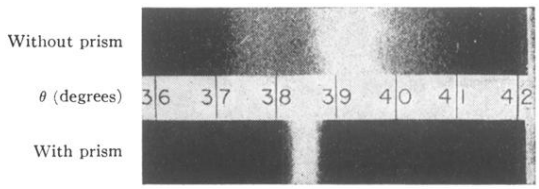

FIG. 4. Positive prints showing Čerenkov radiation as a function of an angle. Top—with equipment of Fig. 3. Bottom—with equipment of Fig. 7.

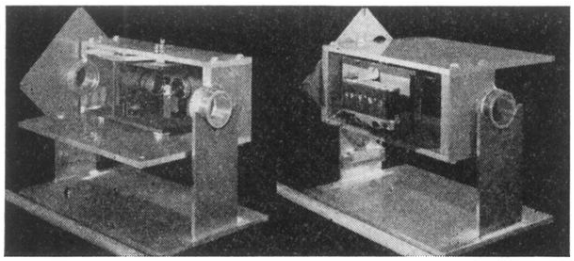

FIG. 8. Energy measuring instrument. Left—normal position (aluminum foil removed from the light tight box of Fig. 8 to show interior construction). Right—inverted position.

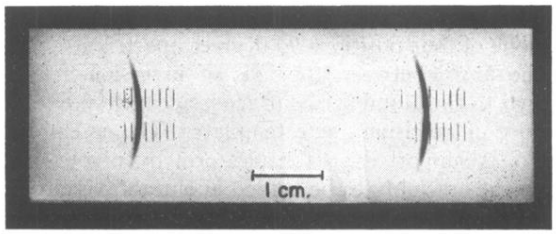

FIG. 9. A pair of Čerenkov images from which the beam energy may be determined (negative print).